Applied Ocean Research 73 (2018) 179–189

Contents lists available at ScienceDirect

Applied Ocean Research

journal homepage: www.elsevier.com/locate/apor

Effect of scour on the structural response of an offshore wind turbine supported on tripod foundation

Hongwang Ma[a,*], Jun Yang[a,b], Longzhu Chen[a]

[a] School of Naval Architecture, Ocean and Civil Engineering, Shanghai Jiao Tong University, Shanghai, China
[b] Department of Civil Engineering, The University of Hong Kong, Hong Kong, China

ARTICLE INFO

Article history:
Received 25 November 2017
Received in revised form 15 January 2018
Accepted 8 February 2018

Keywords:
Offshore wind turbine
Tripod foundation
Scour
Pile
Finite element model

ABSTRACT

A simplified scour model for tripod foundation taking into account both local scour and global scour is proposed in this paper. The model is incorporated into a three-dimensional (3D) finite element model for analysis of a full-scale offshore wind turbine founded on a tripod structure using realistic structural properties. Applicability of the 3D finite element model is validated using full-scale load test data. Four different scour conditions under two wave situations are examined for the ultimate limit state (ULS), serviceability limit state (SLS) and fatigue limit state (FLS). The results show that scour has a minor effect on the natural frequency of the tripod-supported wind turbine but can significantly increase the maximum cross-sectional von Mises stress of piles under the ULS and increase the deflection of piles within nearly 20 m below the original seabed under the SLS. As for the fatigue life of the tripod structure, it can also be reduced by the effect of scour. These findings provide insights which are useful for development of safe and economic design of offshore wind turbines supported by tripod foundations.

1. Introduction

Engineers who plan and design wind turbines in offshore environment need to deal with scouring phenomena around the foundations for wind turbines [1,2]. Scour is the result of erosion of soil particles at and near a submerged foundation and is caused by waves and current. Scour can be regarded as a load effect and may have an impact on the capacity of the foundation and thereby on the response of the structure supported by it [3]. At present, most of the installed wind turbines in the world are supported by monopiles, and much work has been carried out to investigate the scour effect associated with monopile foundations [4–9]. Several methods have been proposed to estimate the maximum scour depth, the maximum scour extension and the development of scour depth over time [3,10]. These methods have been examined using full-scale measurements from nearly ten European offshore wind farms [4]. The examination showed that the maximum scour depth was less than the estimated for most wind farms [4,6]. The effect of scour on the natural frequency of a full-scale wind turbine with monopile foundation over a range of soil densities was studied using a numerical method [11], and it was found that the wind turbine in loose sand would exhibit the largest reduction in natural frequency resulting from scour.

For wind turbines with large capacity (>5 MW) and installed in deep waters (>30 m), monopile foundation is not considered economically viable or technically feasible [12]. Space-frame support structures such as tripod, tripile or jacket are feasible alternatives. Among these structures, a tripod structure is a three-legged steel structure which can provide good stability and stiffness to the entire system [13,14]. The tripod foundation has been used in three wind farm projects, namely Alpha Ventus, Trianel Windpark Borkum and Global Tech I Windfarm of Germany [12,15]. This type of foundation will also be used in Binhai and Dongtai offshore wind farms of Jiangshu province in China [16]. Due to the complexity of tripod structures, there are significant gaps in the knowledge of scour initiation and progression and their effects on stability of the structures. This knowledge is however important for the development of safe and cost-effective design of large offshore wind turbines [17]. Currently there is a rather limited number of studies concerning the effect of scour on tripod structures [2,17]. A recent notable one is that of Stahlmann [17], in which the possible influencing factors on scour progression for a tripod structure were investigated using physical model tests in wave flumes and using CFD based numerical simulations. A comparison with in-situ measured scour data [19] showed overall good agreement.

* Corresponding author.
E-mail address: hwma@sjtu.edu.cn (H. Ma).

https://doi.org/10.1016/j.apor.2018.02.007
0141-1187/

Nomenclature

The following symbols are used in this paper

A^z_{tower}	Wind pressure area on the tower of height z
C_D	Drag coefficient
C_M	Mass coefficient
C_s	Shape coefficient
C_T	Thrust coefficient
d_w	Water depth
D_{bb}	Diameter of the base
D_{bt}	Diameter of the brace
D^b_{mc}	Diameter of bottom segment of the main column
D^m_{mc}	Diameter of middle segment of the main column;
D^t_{mc}	Diameter of top segment of the main column
D_p	Diameter of the pile
D_s	Diameter of the sleeve
E_p	Young's modulus of steel
E_s	Young's modulus of the soil
$F_{current}$	Horizontal current drag force per unit length
F_D	Drag force
F_M	Inertia force
F^Z_{tower}	Wind load acting on the tower of height z
F_{vh}	Wind load acting on the hub
g	Acceleration of gravitation
h_w	Wave height
k	Wave number
r_b	Base radius of the tripod foundation
r_c	Radius of the lowermost main column
r_p	Radius of the tripod piles
r_{sc}	Radius of the scour hole under the main column
r_{sp}	Radius of the scour hole of the tripod piles
R_T	Rotor radius
S_c	Equilibrium scour depth under the main column
S_G	Global scour depth
S_p	Equilibrium scour depth of tripod piles
t_{bb}	Base wall thickness
t_{bt}	Brace wall thickness
t^b_{mc}	Bottom segment wall thickness of the main column
t^m_{mc}	Middle segment wall thickness of the main column
t^t_{mc}	Top segment wall thickness of the main column
t_p	Pile wall thickness
t_s	Sleeve wall thickness
T_w	Wave period
$U_{current}$	Local current velocity
V_{hub}	Wind speed at the hub height
V_z	Wind profile
z	Height above the sea water level
z_2	Depth below sea surface
α	Power law exponent
c'	Cohesion
ϕ'	Friction angle
λ_p	Unit weight of steel
ρ	Mass density of the sea water
ρ_a	Air density
γ'	Density of the soil
ψ'	Dilation angle
ν_p	Poisson's ratio of steel
υ'	Poisson's ratio of the soil
$\dot{x}$	Wave induced velocity of water
$\ddot{x}$	Wave induced acceleration of water
$\eta(t)$	Surface wave profile
w_w	Wave frequency
$\Delta\sigma_{eq}$	Equivalent stress range due to wind and wave loads
$\Delta\sigma_{wind}$	Stress range due to wind load
$\Delta\sigma_{wave}$	Stress range due to wave load
FLS	Fatigue limit state
SLS	Serviceability limit state
ULS	Ultimate limit state

In this paper, a simplified scour model including both local and global scour for tripod foundation is proposed based on the test results of Stahlmann [17] and field scour measurements for a tripod foundation in the Alpha Ventus wind farm [18]. This scour model is then incorporated in a three-dimensional (3D) finite element model for a full-scale offshore wind turbine founded on a tripod structure in which realistic structural properties for a 6 MW wind turbine are adopted. The applicability of the finite element model is validated against experimental results. The effect of stiffness and capacity of the foundation and the natural frequencies of the wind turbine system are investigated. Design implications for tripod foundations against scour are suggested.

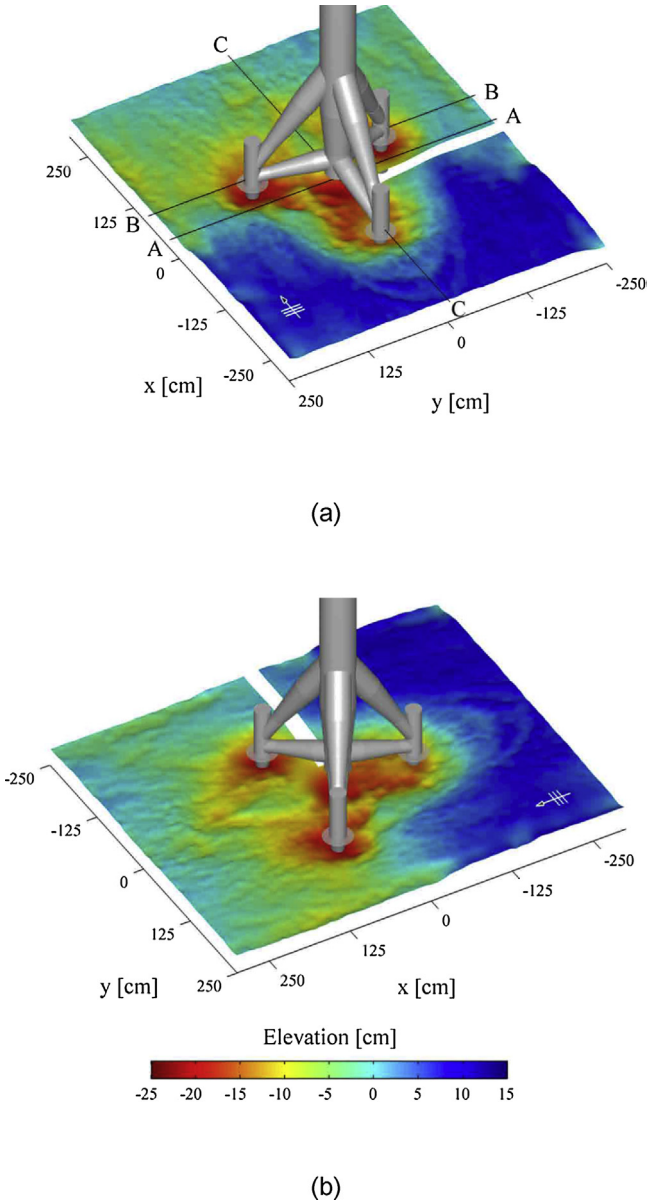

Fig. 1. Results of scour development from test series r7655-01 after 3000 wave cycles [17]: (a) front view; (b) rear view.

2. Modeling of scour at tripod foundations for offshore wind turbine

2.1. Overall scour pattern

Modeling of scour at tripod foundations for offshore wind turbines is inspired by model test results [17] and in-situ measured scour data at Park Alpha Ventus in the German North Sea [17,18]. Physical model tests carried out by Stahlmann [17] in wave flumes included two different scales: 1:40 and 1:12. Different wave load conditions and wave-encounter angles were investigated in both model setups, and the general processes of scour progression and the final scour pattern were provided. The main result of the investigation, as shown in Fig. 1, was that the scour formation around the tripod foundation differs significantly from the scour patterns observed at single vertical monopile foundation.

Furthermore, field scour measurements at a tripod foundation in the Alpha Ventus test site were conducted by the German Federal Maritime and Hydrographic Agency (BSH) [18]. The collection was carried out by use of single beam echo sounders installed around the piles and underneath the central tube and by measuring campaigns using ship-based multi-beam echo sounder collections of the surrounding sea floor in the immediate vicinity of the structure [18,19]. The overall scour pattern and the depth of in-situ detected scours show good agreement with the physical model test results, which are summarized as follows and schematically shown in Fig. 2:

(a) Local scour occurs at each of the tripod piles, with larger depth at the rear pile. The ratios of the maximum scour depths between the front pile and the rear pile are 0.66 and 0.69 in the 1:40 scale experiments, 0.56 and 0.71 in the 1:12 scale experiments, and 0.53–0.77 for the in-situ measurements.
(b) Scour also occurs beneath the main column of the tripod structure. The maximum scour depth $\frac{S_c}{r_c}$ reaches 0.88 in the 1:40 scale experiments, 1.26 and 1.62 in two tests in the 1:12 scale experiments and 3.0 in the in-situ measurements. Here s_c is the equilibrium scour depth under the main column and r_c is the radius of the lowermost main column.
(c) Global scour occurs around the entire tripod structure, with the scour depth of about 0.8 m [18].

2.2. Modeling of scour at tripod foundations

Based on physical model test results and field observations [17,18], the following three assumptions are made in establishing the scour model for which the parameters are estimated using Eqs. (1)–(5).

(a) The local scour depth and the lateral extension of scour hole around the piles can be calculated as that for single piles [3], with four local scour conditions:
  (1) Condition 1: No scour occurs.
  (2) Condition 2: The scour depth is uniform around tripod piles and reaches the equilibrium scour depth S_p.
  (3) Condition 3: For wave direction 1, the scour depths of pile2 and pile3 (rear piles) reach the equilibrium scour depth S_p, while the scour depth of pile1 (front pile) is assumed to be 60% of that for rear piles.
  (4) Condition 4: For wave direction 2, the scour depth of pile 1 (rear pile) reaches the equilibrium scour depth S_p, while the scour depths of pile2 and pile3 (front piles) are assumed to be 60% of that for the rear pile.

Table 1
Properties of 6 MW offshore wind turbine [22].

Property	Value
Rating	6 MW
Hub height	100 m
Rotor radius	80.35 m
Cut-in wind speed	3.0 m/s
Nominal wind speed	10.5 m/s
Cut-out wind speed	25.0 m/s
Nacelle mass	230 t
Rotor mass	95 t
Blade mass	29 t
Nacelle rotational inertia transverse direction (J) (kg.m^2)	2.5×10^7
Nacelle rotational inertia fore-aft direction (J) (kg m^2)	3.5×10^7

Table 2
Tower dimensions.

Height above MSL	Wall thickness (m)	Diameter (m)
10 (flange 10 m above MSL)	0.054	6.0
14	0.04	6.0
17	0.038	5.9
24.5	0.036	5.757
36	0.034	5.61
57	0.032	5.334
65	0.03	5.226
74	0.28	5.117
86	0.026	4.93
87.25	0.03	4.8

(b) The maximum depth of scour hole under the main column is assumed to be $3r_c$. The lateral extent of the scour hole under the main column is calculated according to Eq. (4) [18].
(c) The global scour is assumed to consist of an overall lowering of the seabed around the entire tripod structure, and the maximum global depth is assumed to be $0.7r_p$ [18,20,21].

$$S_p = 2.6r_p \tag{1}$$

$$r_{sp} = r_p + \frac{S_p}{tan\varphi} \tag{2}$$

$$S_c = 3.0r_c \tag{3}$$

$$r_{sc} = r_c + \frac{S_c}{tan\varphi} \tag{4}$$

$$S_G = 0.7r_p \tag{5}$$

where S_p is the equilibrium scour depth of tripod piles; r_p is the radius of the tripod piles; r_{sp} is the radius of the scour hole of the tripod piles; S_c is the equilibrium scour depth under the main column; r_c is the radius of the lowermost main column; r_{sc} is the radius of the scour hole under the main column; φ is the friction angel of the soil; S_G is the global scour depth.

3. Wind turbine, foundation and loads

3.1. Wind turbine and foundation

A 6 MW reference wind turbine from the National Basic Research Program of China [22] is considered. The wind turbine is supported on an annular tower, which is founded on a tripod foundation embedded 40 m in sand. The base radius is r_b = 15 m and the water depth is 30 m. Fig. 3 shows a schematic of the reference wind turbine and its tripod foundation. Details of the wind turbine properties are outlined in Table 1. The geometric properties of the tripod foundation are shown in Fig. 4. The dimensions of the tower are listed in Table 2. As shown in Fig. 5, a uniform sand deposit of 40 m is assumed and typical sand parameters encountered in the offshore environment are adopted [23,24].

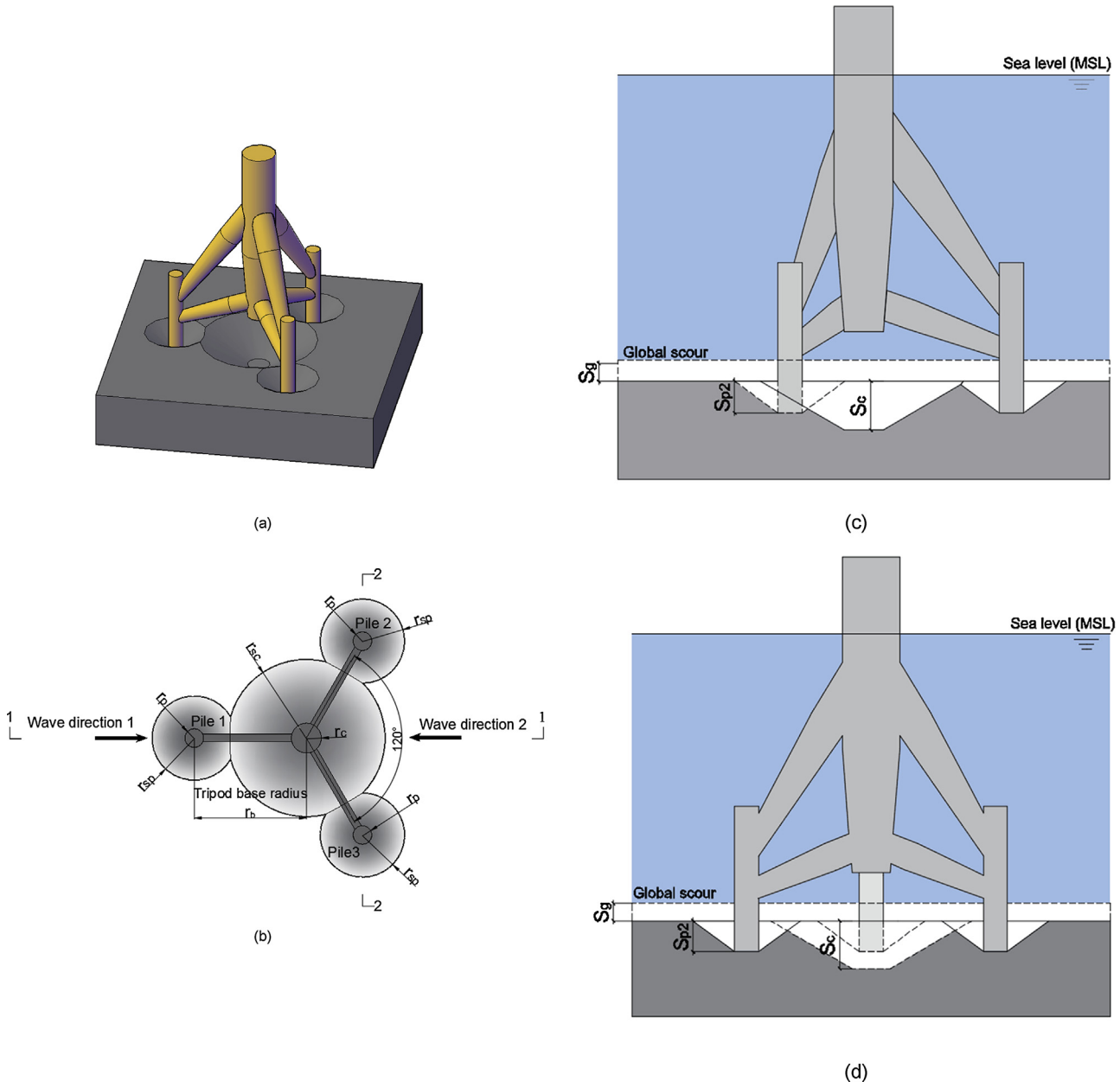

Fig. 2. Scour model of tripod foundation: (a) extent of scour holes around tripod piles; (b) plan view of the scour model; (c) 1–1 section view of the scour model; (d) 2–2 section view of the scour model.

3.2. Loads on structure

The offshore environment includes external loads by wind, waves and current while the weight of the wind turbine and the weight of the support structure lead to gravitational loads.

3.2.1. Wind loads

Wind-generated loads on the rotor and the tower shall be considered. The load acting on the turbine rotor is estimated as [25,26]:

$$F_{vh} = 0.5(\rho_a/g)R_T^2 V_{hub}^2 C_T \tag{6}$$

where F_{vh} is the wind load acting on the hub in N, R_T is the rotor radius in m, V_{hub} is the wind speed at the hub height in m/s, ρ_a is the air density which equals to 12.3 N/m^3, g is the acceleration of gravitation in m/s^2, C_T is thrust coefficient which is a function of the tip speed ratio, approximately considered as 0.16 for $V_{hub} = 25m/s$ and 0.5 for $V_{hub} = 10.5$ m/s in the present study.

The wind load acting on turbine tower depends on wind velocity along the tower. The tower is divided into different segments and wind load acts as a concentrated load at each segment. The wind load acting on the tower is calculated according to [27]:

$$F_{tower}^Z = 0.5\left(\frac{\rho_a}{g}\right) C_s A_{tower}^z V_z^2 \tag{7}$$

where F_{tower}^Z is the wind load acting on the tower of height z in N; A_{tower}^z is the wind pressure area on the tower of height z in m^2; C_s is shape coefficient which equals to 0.5 for the tubular steel tower; ρ_a is the air density which equals to 12.3 N/m^3, g is the acceleration of gravitation in m/s^2, z is the height above the sea water level. The wind profile, V_z, denotes the average wind speed as a function of height z; in the case of standard wind turbines, the normal wind speed profile is given by the power law [27]:

$$V_z = V_{hub}\left(\frac{z}{z_{hub}}\right)^{\alpha} \tag{8}$$

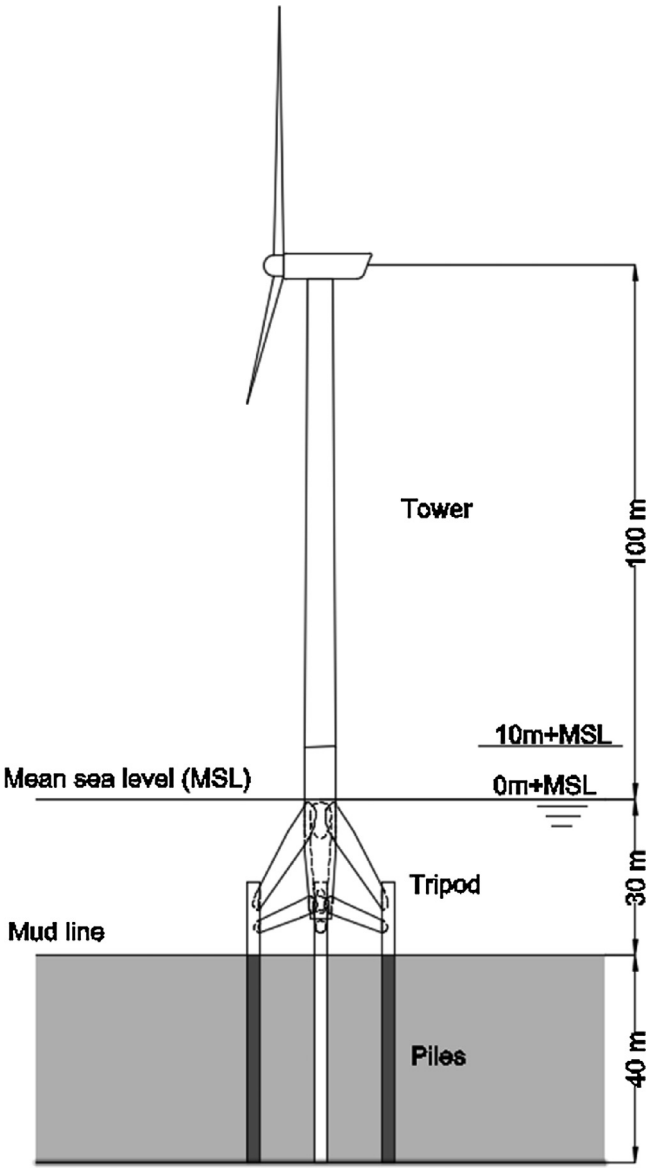

Fig. 3. Schematic of a 6 MW wind turbine and its tripod foundation.

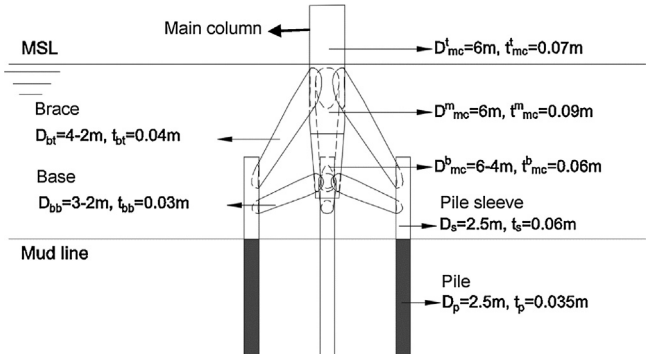

Fig. 4. Geometric properties of the tripod foundation.

where z_{hub} is the height of the hub; α is the power law exponent which is assumed to be 0.2.

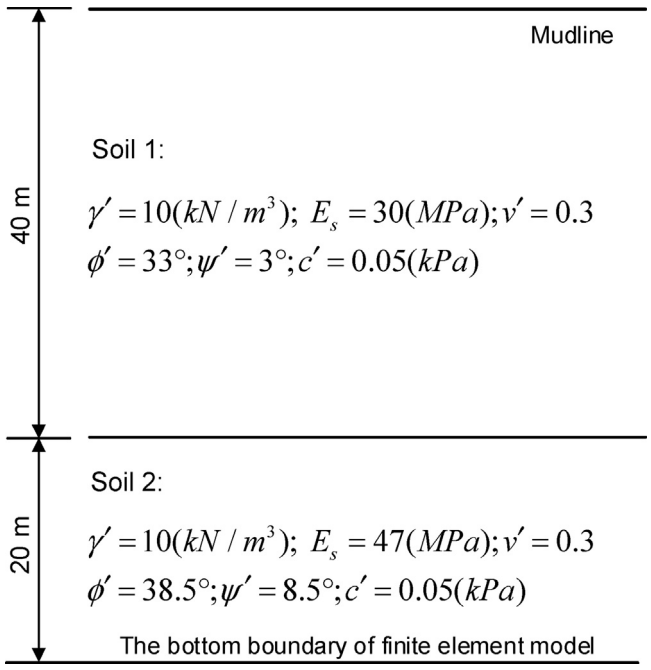

Fig. 5. Soil profiles and parameters.

3.2.2. Wave and current loads

Wave loads on the slender structural members, such as a cylinder submerged in water, can be predicted by Morison's equation [3,28].

$$F_{wave} = F_M + F_D = \int_{-d_w}^{\eta(t)} C_m \rho \pi \frac{D^2}{4} \ddot{x} dz + \int_{-d_w}^{\eta(t)} C_D \rho \frac{D}{2} \dot{x}|\dot{x}| dz \tag{9}$$

where F_M is the inertia force in N; F_D is the drag force in N; d_w is the water depth in m; C_M is the mass coefficient (2 for a smooth tubular section); C_D is the drag coefficient (1.2) for a smooth tubular section; ρ is the mass density of the sea water (1030 kg/m^3); D is the diameter of the each section of tripod foundation in m; $\dot{x}$ and $\ddot{x}$ are the wave induced velocity and acceleration of water, respectively in the horizontal direction, and $\eta(t)$ is the surface wave profile. The surface wave profile according to linear wave theory is given by [28]:

$$\eta(t) = 0.5 h_w \cos(kx - w_w t) \tag{10}$$

$$\dot{x} = \frac{h_w}{T_w} \frac{\pi \cosh(k(z_2 + d_w))}{\sinh(kd_w)} \cos(kx - w_w t) \tag{11}$$

$$\ddot{x} = \frac{2 h_w \pi^2}{T_w^2} \frac{\cosh(k(z_2 + d_w))}{\sinh(kd_w)} \sin(kx - w_w t) \tag{12}$$

where h_w is the wave height in m; k is the wave number in m^{-1}, w_w is the wave frequency in rad/s, T_w is the wave period in s; z_2 is the depth below sea surface in m.

Current models for structural design usually involve a simple current profile over depth, using the known current velocity at the water surface as an input parameter. A commonly used method – the power law profile – is adopted here [27]. The horizontal current load is estimated as:

$$F_{current} = C_D \rho \frac{D}{2} U_{current} \tag{13}$$

where $F_{current}$ is the horizontal current drag force per unit length in N; $U_{current}$ is the local current velocity in m/s.

Other sources of dynamic loads on tripod foundation due to break waves, ice and earthquakes are not considered in this study.

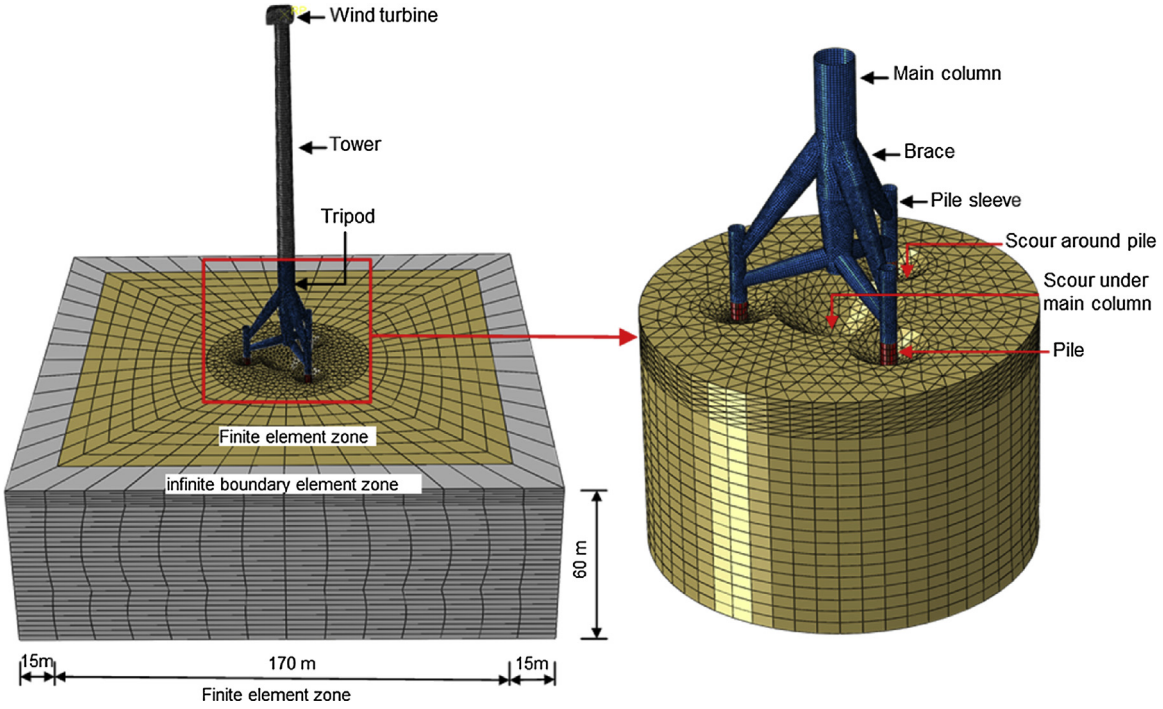

Fig. 6. 3D finite element model constructed for analysis.

3.3. Fatigue loads

Fatigue loads are caused by continuous stress differences in a structural component. Components of the offshore wind turbine system is generally designed to sustain up to design service life 20–25 years, leading to fatigue cycles of 10^7–10^8 [25]. The time domain simulation of complete turbine dynamics requires a significant amount of computational effort [5]. In the present study, two loads are considered for fatigue: mean wind load and mean wave load. Therefore, the equivalent stress range of combined mean wind and wave loads with the same direction can be approximated as [29]:

$$\Delta\sigma_{eq} = \sqrt{\Delta\sigma_{wind}^2 + \Delta\sigma_{wave}^2} \tag{14}$$

where $\Delta\sigma_{eq}$ is the equivalent stress range due to wind and wave loads; $\Delta\sigma_{wind}$ is the stress range due to wind; and $\Delta\sigma_{wave}$ is the stress range due to wave.

Only global fatigue analysis in the most critical cross section is considered in this study. The fatigue life for steel of the offshore wind turbine system is estimated with the S-N curve [3].

$$log_{10}^{N_{eq}} = log_{10}^{a} - mlog_{10}\left(\Delta\sigma_{eq}\left(\frac{t}{t_{ref}}\right)^{k}\right) \tag{15}$$

where N_{eq} is fatigue life, i.e. number of stress cycles to failure at the stress range $\Delta\sigma_{eq}$; m is negative slope of S-N curve on the $\mathrm{Log^N} - \mathrm{Log^S}$ plot and $m = 5$ for $N_{eq} > 10^6$; $log_{10}^{N_a}$ is the intercept of $log_{10}^{N_{eq}}$ and $log_{10}^{a} = 15.6$ for $N_{eq} > 10^6$; t_{ref} is reference thickness, $t_{ref} = 32$ mm for tubular joints, $t_{ref} = 25$ mm for welded connections; t is thickness through which the potential fatigue crack will grow, and $t = t_{ref}$ shall be used when $t < t_{ref}$; k is thickness exponent, also known as scale exponent which is taken as 0.25 [3,30].

4. 3D finite element model and verification

Fig. 6 shows a three-dimensional (3D) finite element model for the tripod supported wind turbine system established using ABAQUS [31]. The key geometric parameters are summarized in Figs. 2 and 3, Tables 1 and 2.

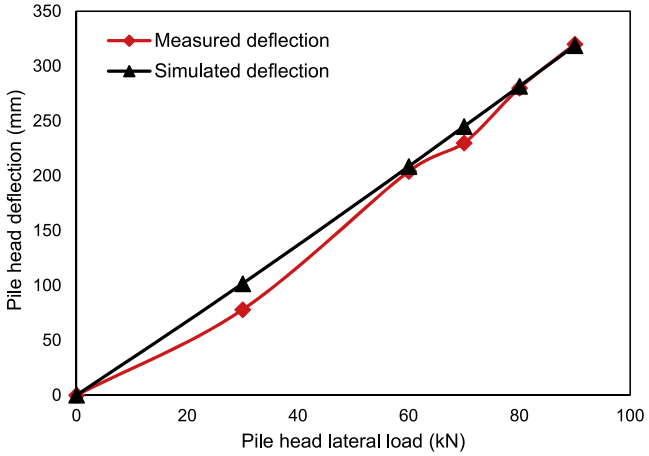

Fig. 7. Comparison of test results and numerical simulation results.

4.1. Geometric configuration

The size of the soil domain in the finite element model is $200 \times 200 \times 60$ m [32]. The bottom boundary is fixed against movements in all directions, and the 15 m thick layer of infinite soil is to create vertical boundaries which would not reflect shear waves in the soil medium. The continuum element type (C3D8R) is used to model the soil. The outer layer of soil is modeled using a single layer of solid infinite element (CIN3D8). The tower, tripod foundation and piles are modeled using shell elements (S4R). The nacelle is modeled as a lumped mass at the top node of the tower with a rotational inertia as specified in Table 1, with the contribution from the mass of the rotor and the blades.

Table 3
Comparison of the natural frequency between FE analysis and field tests.

FEM	Measurements	
	Over speed stop	Ambient excitation
0.3657 Hz	0.3529 Hz	0.3565 Hz

4.2. Material model and properties

The soil is represented by a Mohr-Coulomb constitutive model with elastic-perfectly plastic behavior. The elastic-plastic behavior is mainly defined by cohesion, internal friction angle, dilation angle, modulus of elasticity and Poisson's ratio as shown in Fig. 5. The pile, tripod foundation and tower are assumed to be made of steel material which has typical properties of Young's modulus, $E_p = 2.1 \times 10^5$ MPa, Poisson's ratio $\nu_p = 0.3$ and unit weight $\lambda_p = 78$ kN/m^3. Yielding of the steel is not considered in this study.

4.3. Interaction properties

The interface between the soil and the pile is simulated by the coulomb friction law, and detachment between the pile and the surrounding soil is allowed [33]. Tangential behavior is considered to be governed by penalty interaction with the frictional coefficient at the interface simply taken as 2/3 of the friction angle of the surrounding soil. Normal behavior is defined by the contact pressure-over-closure relationship [33].

In the FE analysis the initial soil stresses due to gravity are calculated by application of gravity loading. The natural frequency is calculated using the linear perturbation procedure in ABAQUS, while the structural response under wave and wind loads is calculated by the general static method.

4.4. Feasibility of finite element model

Hokmabadi et al. (2012) reported full-scale load tests to investigate the behavior of offshore monopiles in marine sandy soil [34]. The length and diameter of the monopile were approximately 40 m and 2 m, respectively. A 3D finite element model similar to the one developed in the present study was established using ABAQUS for this monopile-supported wind turbine, with the properties of the soil and pile taken from [34]. The result of pile head load versus pile head deflection obtained from the finite element analysis is presented in Fig. 7, showing a reasonably good agreement.

Shirzadeh et al. (2013) reported real life measurements of the first for-aft mode frequency for a 3 MW offshore wind turbine supported by a monopile in the Belgian North Sea [35]. The over speed stop test and ambient excitation were used to estimate the first for-aft mode frequency. Based on the available soil, monopile, tower and turbine data from [35], a 3D finite element model was developed using ABAQUS. Table 3 presents the result from the finite element analysis and the measurement for the first for-aft mode frequency, showing good agreement.

Table 6
Wave and current loads for ULS, SLS and FLS.

Loads		ULS	SLS	FLS
Wave loads (kN)	Main Column	1663.6		2017.3
	Brace	180.5		171
	Base	37.97		0.984
	Pile sleeve	70.0		2.583
Current loads (kN)	Main Column		153	
	Brace		55.2	
	Base		30.7	
	Pile sleeve		12.7	

5. Numerical results

5.1. Loading conditions

In design and analysis of offshore wind turbines, several load combinations need to be investigated, including the ultimate limit state (ULS), serviceability limit state (SLS) and fatigue limit state (FLS). Table 4 presents the environmental site conditions considered in this study.

The wind load is applied to the finite element model (see Fig. 6) at tower top. The tower is divided into five segments and the wind load acts as a concentrated load at each segment. The wave load and current load per unit length are calculated using Eqs. (1) and (2), respectively, and they are assumed to act as uniform load on the surface of the tripod foundation. In this study, the water depth is assumed to be 30 m, and the wave velocity is relatively low at the mudline. Therefore, the total wave and current loads on the segments of piles in the scour zone are relatively small compared

Table 4
Environmental site conditions.

Load conditions	Value			
	ULS	SLS	FLS	
Water depth (m)	30	30	30	
10-min average hub height wind speed (m/s)	25	10.5	Average wind speed (m/s)	10.5
			Turbulence intensity	0.12
Current velocity (m/s)	1	1	1	
Wave height (m)	6	6	1.26	
Peak spectral wave period (s)	8.65	8.65	3.95	

Table 5
Wind loads for ULS, SLS and FLS.

Loads			ULS	SLS	FLS	
	Position	Point of wind load from sea level (m)			Up	Down
Wind load (kN)	Hub	100	1246.7	687.2	862.1	532.2
	Tower	90	19.2	3.4	4.25	2.63
		70	17.5	3.1	3.89	2.40
		50	15.2	2.76	3.47	2.14
		30	13.3	2.34	2.95	1.82
		10	10.1	1.78	2.23	1.38

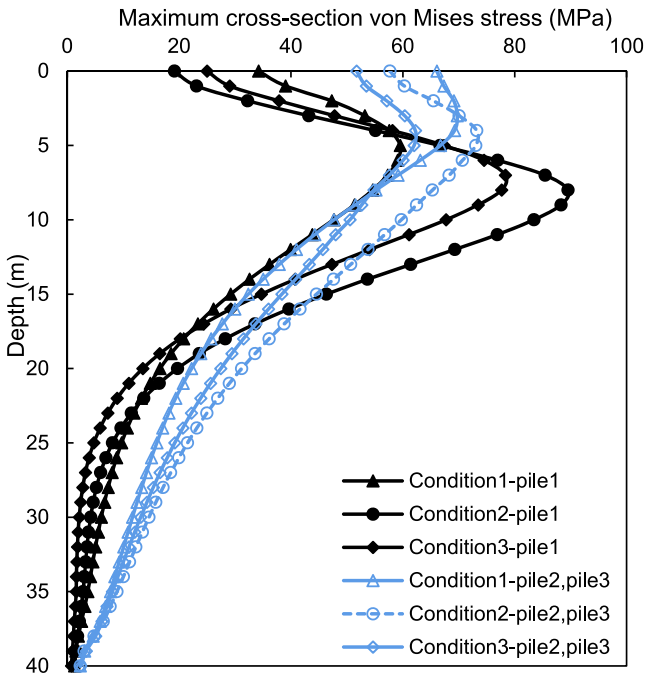

(a) Wave direction 1

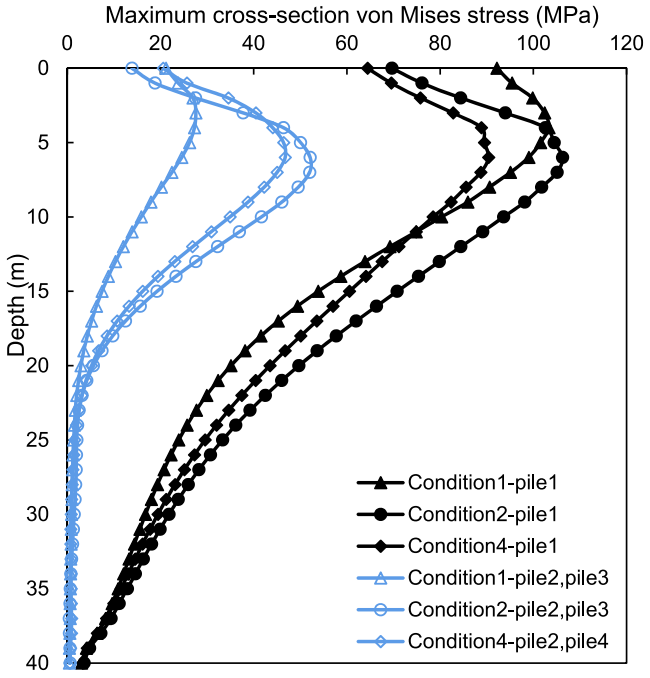

(b) Wave direction 2

Fig. 8. Distribution of maximum cross-sectional von Mises stress in piles under ULS.

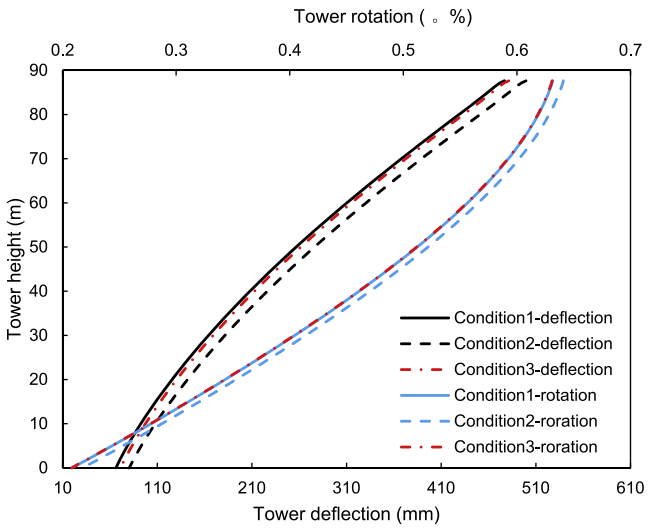

(a) Wave direction 1

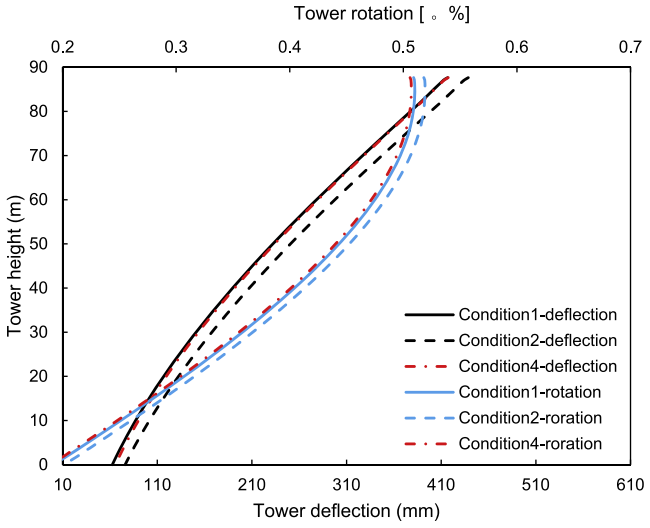

(b) Wave direction 2

Fig. 9. Distribution of deflection and rotation in tower under SLS.

with the total wave and current loads on the tripod foundation in water. Moreover, because the wave and current loads on the segments of piles in the scour zone are complicated, no reliable formula are available for calculation of the loads. Therefore, the differences between pre-scour and post-scour conditions are not considered. The estimated wind and wave loads for ULS, SLS and FLS are summarized in Tables 5 and 6.

5.2. Natural frequency

The natural frequency is an important design consideration for offshore wind turbines [36]. For conventional offshore wind turbines, avoidance of resonance is often achieved by using the soft-stiff design approach where the resonance frequency is in the range between the rotor frequency (1P) and the blade passing frequency (3P) [37]. The rotor speed of the wind turbine in this study is 6–12 rpm, and hence the first natural frequency should lie between 0.2–0.3 Hz. The frequency is calculated using the linear perturbation procedure in ABAQUS/Standard. The first and second frequencies are obtained by matching their vibration modes, as shown in Table 7 for various conditions (i.e. fixed base at mudline, Conditions 2, 3, 4 for scour and Condition 1 for no scour). The first natural frequency for Condition 4–1 varies from 0.2807 Hz to 0.2847 Hz. Compared with the 1P frequency of 0.2 Hz and the 3P frequency of 0.3 Hz, the entire system safely lies in the soft-stiff range. The assumption of fixed base at mudline overestimates the

Table 7
Calculated natural frequencies under different conditions (Hz).

Frequency (Hz)	Fixed base at mudline	Conditon-1	Condition-2	Conditon-3	Condition-4
The first natural frequency	0.312	0.2847	0.2807	0.2818	0.2822
The second natural frequency	2.1687	1.486	1.4547	1.4581	1.4643

first natural frequency by 9.58% for Condition 1, 11.2% for Condition 2, 10.7% for Condition 3 and 10.5% for Condition 4, respectively. The change in first natural frequency due to different scour conditions is approximately 0.9–1.4%, while the change in second frequency is about 1.5-2.1%. Sørensen and Ibsen [5] and Prendergast et al. [11] investigated the effect of scour on the first natural frequency of monopile-supported wind turbines and found that the first natural frequency would decrease by about 5% to 8.5% due to the scour effect. This implies that the effect of scour on the natural frequency of wind turbines supported by tripod foundations is slight as compared with that for wind turbines supported by monopiles.

5.3. ULS design

For ULS design conditions, the wind, wave and current loads applied are summarized in Tables 5 and 6. The maximum cross-sectional von Mises stresses of piles for wave directions 1 and 2 under various scour conditions are shown in Fig. 8(a) and (b). In the case of wave direction 1, scour causes a significant increase in the maximum cross-sectional von Mises stresses of pile 1. The location of the maximum cross-sectional von Mises stress is also affected by scour, varying from about 5 m below the seabed without the effect of scour (Condition 1) to about 8 m under the scour condition 2. Compared with pile 1, the effect of scour is relatively small for piles 2 and 3 for both the magnitude and location of the maximum cross-sectional von Mises stress.

The computed axial loads of piles under different scour conditions are listed in Table 8. For each scour condition, two loading cases are considered in the analysis: one is that horizontal loads due to wind and waves are included and the other is that the horizontal loads are excluded (i.e. only the gravity load included). It is worth noting that the axial load of pile 1 will change from compression to tension when horizontal loads are included in the analysis, while the axial compression loads of pile 2 and pile 3 are nearly doubled. The effect of scour is to increase the axial load by about 5% for all piles. In the case of wave direction 2, the effect of scour is to increase the maximum cross-sectional von Mises stresses of piles 2 and 3; the location of the maximum stress is also affected by scour, varying from 3 m below the seabed (Condition 1) to 6 m below the seabed for Condition 2. Table 9 summarizes the results for axial loads in piles under different scour conditions. Note that there are no tension axial loads in all piles when horizontal loads due to wind and waves are included, but there is a significant increase in axial load of pile 1, from about 5500 kN to 14500 kN.

5.4. SLS design

For SLS design conditions, the deformation tolerances cannot be exceeded [3], particularly the maximum deflection and rotation at pile head and at the nacelle level [38]. The deformation tolerances are typically set based on turbine manufacturer requirements [39]. For example, DNV code specifies the deflection limiting value of 0.5° at the seabed for monopiles [3]. Though there are not deformation tolerances for tripod foundation in current design codes [3,10], it is necessary to examine the deformations of support structures under different scour conditions. Fig. 9(a) shows computed deflection and rotation of the tower in the case of wave direction 1, while Fig. 9(b) shows the results in the case of wave direction 2. For both wave directions, the maximum deflection at the nacelle level is about 0.51 m, and the effect of scour is insignificant.

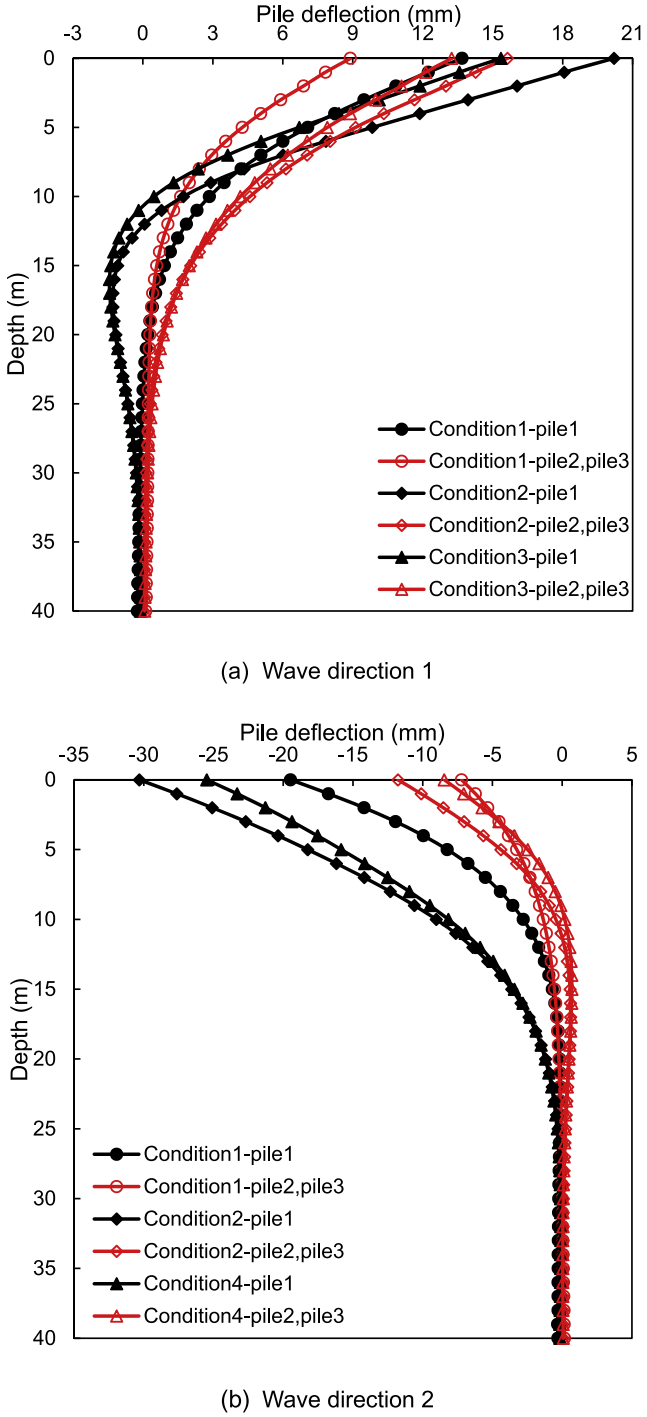

Fig. 10. Distribution of pile deflection under SLS.

Fig. 10(a) and (b) shows the deflection of piles for the cases of wave direction 1 and 2, respectively. It is noted that scour increases the maximum pile deflection for both wave directions and the effect

Table 8
Axial loads in piles under ULS (wave direction 1).

Condition	Axial load (kN)	Pile1	Pile2	Pile3
Condition-1	only gravity	−5346	−5597	−5597
	Including lateral load	+3647	−10060	−10060
Condition-2	only gravity	−5603	−5859	−5859
	Including lateral load	+3762	−10540	−10540
Condition-3	only gravity	−5613	−5855	−5855
	Including lateral load	+3641	−10480	−10480

Note: +ve Tension load; −ve Compression load.

Table 9
Axial loads in piles under ULS (wave direction 2).

Condition	Axial load (kN)	Pile1	Pile2	Pile3
Condition-1	only gravity	−5346	−5597	−5597
	Including lateral load	−14270	−1125	−1127
Condition-2	only gravity	−5613	−5855	−5855
	Including lateral load	−14960	−1181	−1182
Condition-4	only gravity	−5596	−5863	−5864
	Including lateral load	−14670	−1326	−1326

Note: +ve Tension load; −ve Compression load.

Table 10
Fatigue life in cycles.

Selected points	Condition-1			Condition-2			Condition-3		
	$\Delta\sigma_{wind}$ (MPa)	$\Delta\sigma_{wave}$(MPa)	N_{eq} (10^7)	$\Delta\sigma_{wind}$ (MPa)	$\Delta\sigma_{wave}$ (MPa)	N_{eq} (10^7)	$\Delta\sigma_{wind}$ (MPa)	$\Delta\sigma_{wave}$ (MPa)	N_{eq} (10^7)
HS1	17.5	31.7	1.77	18.8	35.9	0.99	18.7	35.2	1.08
HS2	14.1	35.5	3.27	15.9	40.4	1.18	15.5	40.3	1.20
HS3	11.5	26.6	8.86	11.9	29.5	5.59	11.7	28.8	6.24
HS4	16.6	34.2	3.79	17.1	38.5	2.27	16.3	36.1	3.09

Note: Refer to list of notations for definitions.

is more significant on pile 1. In addition, the deflection of pile 1 in the case of wave direction 2 is significantly larger than that in the case of wave direction 1.

5.5. FLS design

For FLS design conditions, the focus of this study is on the scour effect on the most critical tubular joints of the tripod-supported structure. The most severe fatigue locations [40] include, as shown in Fig. 11, the main column and brace tubular joint (HS1), the base and the main column joint (HS2), the brace and sleeve joint above pile 2 (HS3) and the brace and sleeve joint above pile 1 (HS4). Table 10 presents the fatigue life in cycles of these critical spots due to aerodynamic and hydrodynamic loads under various scour conditions. It can be observed that the fatigue life of the tripod ranges from 1.77×10^7–8.86×10^7 cycles under scour condition 1, 0.99×10^7–5.59×10^7 cycles under scour condition 2, and 1.08×10^7–6.24×10^7 cycles under scour condition 3. The effect of scour is to reduce the fatigue life of the tripod. Among the critical spots, HS1 is the most critical one.

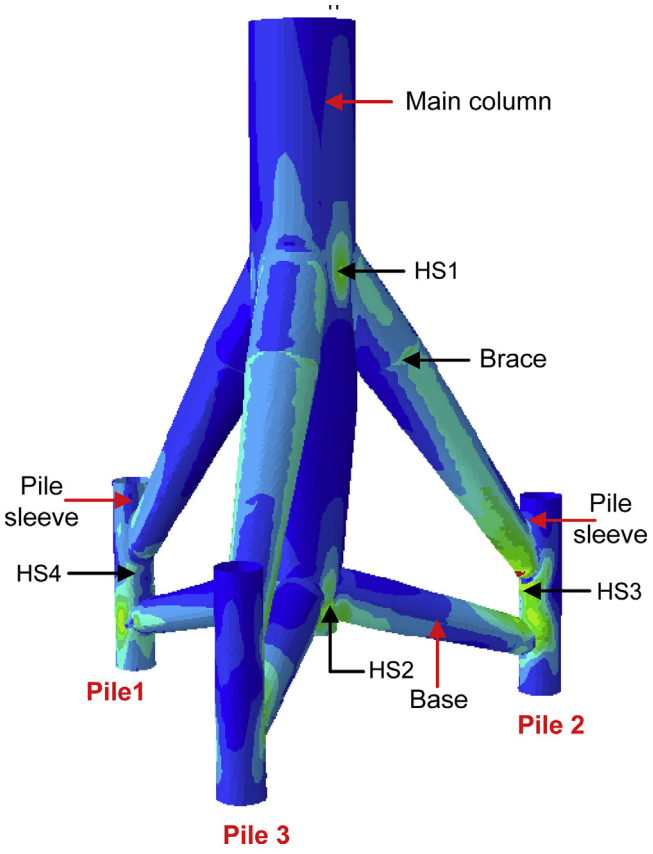

Fig. 11. Location of hotpots.

6. Conclusions

In the design and analysis of offshore wind turbines, the effect of scour on foundations submerged in water is an important issue. This paper presents a numerical study of the scour effect on a full-scale wind turbine supported on a tripod foundation, where four different scour conditions under two wave situations are examined for the ultimate limit state (ULS), serviceability limit state (SLS) and fatigue limit state (FLS). The main results from this study are summarized as follows:

(a) The effect of scour is minor on the natural frequency of the system. The first natural frequency of the system is reduced by about 0.9-1.4% due to scour while the second natural frequency reduced by 1.5 −2.1%.
(b) For ULS design conditions, the effect of scour is significant on both magnitude and location of the maximum cross-sectional von Mises stresses of piles and the effect is affected by wave directions.
(c) For SLS design conditions, the effect of scour is minor on the deflection and rotation of the tower, but it is significant on the deflection of piles.
(d) The effect of scour is to decrease the fatigue life of the tripod foundation, and the main column and brace tubular joint (HS1) is most critical among the fatigue spots examined.

Since the problem concerned is highly complex, future numerical studies investigating different soil, foundation and structure parameters and future physical model tests would be worthwhile in order to develop a more comprehensive understanding of the scour effect on performance of offshore wind turbines.

Acknowledgments

The authors wish to acknowledge the financial support provided by the National Basic Research Program of China (973 Program, No. 2014CB046200) and by the National Natural Science Foundation of China (51428901). The Seed Funding for Basic Research provided by the University of Hong Kong is also acknowledged.

References

[1] T.U. Petersen, Scour Around Offshore Wind Turbine Foundations, Technical University of Denmark, 2014, Ph. D. thesis.
[2] A. Stahlmann, Numerical and experimental modeling of scour at foundation structures for offshore wind turbines, J. Ocean Wind Energy 1 (2) (2014) 82–89.
[3] DNV-OS-J101, Design of Offshore Wind Turbine Structures, DET NORSKE VERITAS, 2014.
[4] R.J.S. Whitehouse, J.M. Harris, J. Sutherland, J. Rees, The nature of scour development and scour protection at offshore windfarm foundations, Mar. Pollut. Bull. 62 (1) (2011) 73–88.
[5] S.P.H. Sørensen, L.B. Ibsen, Assessment of foundation design for offshore monopile unprotected against scour, Ocean Eng. 63 (2013) 17–25.
[6] C. Matutano, V. Negro, J.S. López-Gutiérrez, M.D. Esteban, Scour prediction and scour protections in offshore wind farms, Renew. Energy 57 (2013) 358–365.
[7] W.C. Tseng, Y.S. Kuo, J.W. Chen, An investigation into the effect of scour on the loading and deformation responses of monopile foundations, Energies 10 (8) (2017) 1190.
[8] K.A. Abhinav, N. Saha, Effect of scouring in sand on monopile-supported offshore wind turbines, Mar. Georesour. Geotechnol. 35 (6) (2017) 817–828.
[9] W.G. Qi, F.P. Gao, M.F. Randolph, B.M. Lehane, Scour effects on p-y curves for shallowly embedded piles in sand, Géotechnique 66 (8) (2016) 648–660.
[10] Guideline for the Certification of Offshore Wind Turbines, GL Renewables Certification, Hamburg, 2012.
[11] L.J. Prendergast, K. Gavin, P. Doherty, An investigation into the effect of scour on the natural frequency of an offshore wind turbine, Ocean Eng. 101 (2015) 1–11.
[12] J.H. Koh, E.Y.K. Ng, Downwind offshore wind turbines: opportunities, trends and technical challenges, Renew. Sustain. Energy Rev. 54 (2016) 797–808.
[13] M. Arshad, B.C. O'Kelly, Offshore wind turbine structures: a review, ICE: Proceedings of Institution of Civil Engineers Energy 166 (EN4) (2013) 139–152.
[14] C.T. Akdag, Behavior of closely spaced double-pile-supported jacket foundations for offshore wind energy converters, Appl. Ocean Res. 58 (2016) 164–177.
[15] RAVE Research at Alpha Ventus. Available online: http://rave.iwes.fraunhofer.de/raveResources/welcome/RAVE_Brochure_e_komplett_www.pdf.
[16] W. Feng, Developments and characteristics of offshore wind farms in China, Adv. New Renew. Energy 4 (2) (2016) 152–158.
[17] A. Stahlmann, Experimental and Numerical Modeling of Scout at Offshore Wind Turbines, Leibniz University, Hannover, 2013 (Ph. D. thesis).
[18] B. Stuyts, D. Cathie, Scour assessment and measurement for pile-supported wind turbine foundations, in: Proceedings of the ASME 2013 32nd International Conference on Ocean, Offshore and Arctic Engineering, Nantes, France, 2013, pp. 1–10.
[19] A. Stahlmann, T. Schlurmann, Numerical and experimental modeling of scour at tripod foundations for offshore wind turbines, in: ICSE6, Paris, 2012, pp. 27–31.
[20] B.M. Sumer, K. Bundgaard, J. Fredsøe, Global and local scour at pile groups, Int. J. Offshore Polar Eng. 15 (3) (2005) 204–209.
[21] Y.E. Mostafa, A.F. Agamy, Scour around single pile and pile groups subjected to waves and currents, Int. J. Eng. Sci. Technol. 3 (11) (2011) 8160–8178.
[22] The National Basic Research Program of China (973 Program, No. 2014CB046200) Annual Report, Nan Jing University of Aeronautics and Astronautics, China, 2015.
[23] S.J. Jung, S.R. Kim, A. Patil, L.C. Hung, Effect of monopile foundation modeling on the structural response of a 5-MW offshore wind turbine tower, Ocean Eng. 109 (2015) 479–488.
[24] M. Achmus, Y.S. Kuo, K. Abdel-Rahman, Behavior of monopile foundations under cyclic lateral load, Comput. Geotech. 36 (2009) 725–735.
[25] S. Bisoi, S. Haldar, Dynamic analysis of offshore wind turbine in clay considering soil-monopile-tower interaction, Soil Dyn. Earthquake Eng. 63 (2014) 19–35.
[26] L. Arany, S. Bhattacharya, J. Macdonald, S.J. Hogan, Design of monopiles for offshore wind turbines in 10 steps, Soil Dyn. Earthquake Eng. 92 (2017) 126–152.
[27] ABS Guide for Building and Classing Offshore Wind Turbine Installations, American Bureau of Shipping ABS Plaza, 2010.
[28] W. Nie, Q.Y. Liu, Dynamic Analysis of Offshore Structures, Harbin Engineering University Press, Harbin, China, 2002.
[29] F.V. Gerven, Optimizing the Design of a Steel Substructure for Offshore Wind Turbines in Deeper Waters, TU Delft, Delft, 2011 (MSc. Thesis).
[30] S. Bisoi, S. Haldar, Design of monopile supported offshore wind turbine in clay considering dynamic soil −structure −interaction, Soil Dyn. Earthquake Eng. 73 (2015) 103–117.
[31] Sam Helwany, Applied Soil Mechanics: with ABAQUS Applications, John Wiley & Sons, Inc., 2007.
[32] Y. Kim, S. Jeong, Analysis of soil resistance on laterally loaded piles based on 3D soil-pile interaction, Comput. Geotech. 38 (2) (2011) 248–257.
[33] D. Bhowmik, D.K. Baidya, S.P. Dasgupta, A numerical and experimental study of hollow steel pile in layered soil subjected to lateral dynamic loading, Soil Dyn. Earthquake Eng. 53 (2013) 119–129.
[34] A.S. Hokmabadi, A. Fakher, B. Fatahi, Full scale lateral behaviour of monopile in granular marine soils, Mar. Struct. 29 (2012) 198–210.
[35] R. Shirzadeh, C. Deveriendt, M.A. Bidakhvidi, P. Guillaume, Experimental and computational damping estimation of an offshore wind turbine on a monopile foundation, J. Wind Eng. Ind. Aerodyn. 120 (2013) 96–106.
[36] A.T. Myers, S.R. Arwade, V. Valamanesh, S. hallowell, W. Carswell, Strength, stiffness, resonance and the design of offshore wind turbine monopiles, Eng. Struct. 100 (2015) 332–341.
[37] M. Damgaard, V. Zania, L.V. Andersen, L.B. Ibsen, Effects of soil-structure interaction on real time dynamic response of offshore wind turbines on monopiles, Eng. Struct. 75 (2014) 388–401.
[38] L. Arany, S. Bhattacharya, J.H.G. Macdonald, S.J. Hogan, A critical review of serviceability limit state requirements for monopile foundations of offshore wind turbine, in: Offshore Technology Conference, Houston, Texas, 2015.
[39] S. Bhattacharya, Challenges in design of foundations for offshore wind turbines, Eng. Technol. Ref. 1 (2014) 1–9.
[40] B. Yeter, Y. Garbatov, C.G. Soares, Fatigue damage assessment of fixed offshore wind turbine tripod, Eng. Struct. 101 (2015) 518–528.